Front aggregation in multiarmed excitation vortices

Brent T. Ginn and Oliver Steinbock*
Department of Chemistry and Biochemistry, Florida State University, Tallahassee, Florida 32306-4390, USA
(Received 22 June 2005; published 11 October 2005)

Using the Belousov-Zhabotinsky reaction, we study the pinning of multiarmed spiral waves to nonexcitable obstacles. With increasing obstacle size, the individual arms switch from a repulsive to an attractive state. This transition yields densely aggregated spiral arms and is caused by anomalous dispersion. A kinematic model reproduces the measurements quantitatively and identifies the transition as a supercritical pitchfork bifurcation.

DOI: 10.1103/PhysRevE.72.046109 PACS number(s): 82.40.Ck, 05.45.−a, 82.20.Wt

Rotating spiral waves are a striking example for spatiotemporal self-organization in excitable reaction-diffusion media [1]. These dissipative patterns are known to exist in a broad variety of systems such as catalytic surfaces, single cells, aggregating microorganisms, certain regions of the central nervous systems, and the mammalian heart [2]. Among the most widely studied examples is the chemical Belousov-Zhabotinsky (BZ) reaction [3]. This reaction is also an ideal model for the systematic investigation of excitation waves in media with heterogeneities that are, in various forms, intrinsic to all living matter.

Spiral waves are profoundly affected by the introduction of nonexcitable heterogeneities close to the spiral tip. For obstacles larger than spiral core, one observes simple pinning of the tip to the obstacle's boundary [4]. Smaller obstacles, however, cause complex trajectories and, in the case of periodic obstacle arrays, give rise to quantized spectra of various orbits [5]. The latter situation also introduces an effective anisotropy that affects the overall symmetry of the global wave pattern.

In addition, simple pinning to obstacles alters the rotation period of the wave structure. The period is governed by the dispersion relation $c(\lambda)$, where c and λ denote the propagation velocity of infinite wave trains and the corresponding interpulse distance (i.e., wavelength), respectively. In many chemical and biological systems, the velocity increases monotonically with increasing wavelengths and saturates at a maximal speed c_0 [6]. However, certain media have anomalous dispersion relations that involve a single overshoot, damped oscillations, bistability, or band gaps [7].

Nonmonotonic dispersion relations can be found in excitable systems in which the rest state is a stable focus [8]. Accordingly, an excited medium reapproaches the steady state through damped oscillations that can create a nonmonotonic inhibition profile in the wake of an excitation pulse. In turn, the speed of a trailing pulse shows a nonmonotonic dependence on the distance to its predecessor. Anomalous dispersion can be caused also by the interaction of multiple inhibitors as in the case of wave propagation on Pt(100) surfaces during the catalytic reduction of NO with CO [9].

A similar mechanism seems to be responsible for anomalous dispersion in the 1,4-cyclohexanedione Belousov-Zhabotinsky (CHDBZ) reaction. This particular system shows a variety of intriguing phenomena that affect the dynamics of wave trains and patterns. Examples include accelerating waves, cascade-like reorganizations of pulses in wave trains, pulse annihilation in front-to-back collisions, and the formation of bound pulse multiplets [10]. In this paper, we describe the impact of anomalous dispersion on multiarmed spiral waves in the CHDBZ reaction. To control the rotation period of these patterns, experiments are carried out in periodic obstacle arrays with different obstacle sizes.

Obstacle arrays are produced from polyester casting resin using soft lithography [11]. This material has several advantages over poly(dimethylsiloxane) (PDMS) -based reactors where wave propagation can be affected by a flux of an inhibitory species (Br_2) from the aqueous CHDBZ phase into the PDMS matrix [12]. The first stages of the device fabrication have been described in Refs. [11,12] and yield a silicon wafer that bears the positive surface relief of the desired reactor. We then produce a negative PDMS copy of the relief using silicon elastomer kits (Fisher, Sylgard 184). After curing, the sample is silanized and the procedure is repeated, now with PDMS being poured on PDMS. Using the latter PDMS master, we create the final device from a casting resin and a methyl ethyl ketone peroxide (MEKP) liquid catalyst (TAP Plastics Inc.). The patterned area of the polyester mold is trimmed and holes are drilled to serve as solution reservoirs. The mold is then rinsed with acetone and pressed against a glass surface to achieve thorough bonding. All devices have square obstacles arranged on square lattices. The resulting channels have a constant width of 200 μm and a height of 80 μm.

The devices are filled with the ferroin-catalyzed BZ reaction using 1,4-cyclohexanedione as the organic substrate [13]. Our experiments employ the following initial concentrations (in mol/L): $[H_2SO_4]=2.0$, $[CHD]=0.11$, $[NaBrO_3]=0.07$, $[\text{ferroin}]=5.0\times10^{-3}$. Wave patterns are detected at 488 nm using a charge-coupled-device camera. Video signals are captured with a low-noise frame grabber and commercial software.

To create multiarmed spirals, we exploit the photosensitivity of the reaction medium [13]. We center a circular mask (diameter 5 mm) over the reactor that is populated by spontaneous, high-frequency wave trains. Then we illuminate the system with bright, unfiltered light from a quartz-tungsten-

*Corresponding author. Electronic address: steinbck@chem.fsu.edu

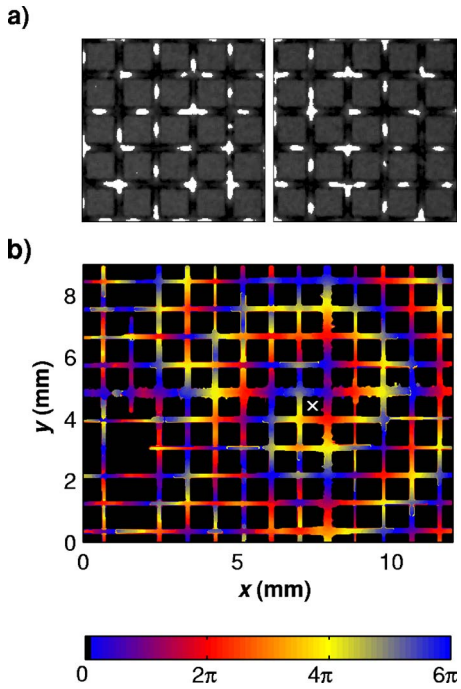

FIG. 1. (Color online) (a) Difference images of a pinned three-armed spiral wave. Spiral tips rotate counter clockwise around the central obstacle. The obstacle width is 0.75 mm and the image area is (4.8×4.8) mm^2. The time elapsed between the two frames is 10 s. (b) Corresponding phase field. The wave fronts are in a repulsive state.

halogen lamp for about 20 s. This perturbation erases all waves except for those located underneath the mask. Along the edge of the unperturbed region, the remaining wave segments begin to rotate around the closest obstacles, thus, creating pinned multiarmed spiral waves.

This procedure yields excitation patterns similar to those shown Fig. 1(a). The individual pulses appear as white dots propagating along a network of dark channels. The detailed dynamics of the pattern are obscured by the strong fragmentation and the large number of front segments. To overcome this problem, we compute a position-dependent phase. First, we measure the local excitation period T (here 20 s). From a sequence of images spanning T, the time of excitation τ is analyzed for each pixel site and linearly scaled to values between 0 and 2π. We then extract the τ values along simple polygons connecting every pixel to an arbitrary reference site and remove phase jumps between 0 and 2π as well as 2π and 4π. Figure 1(b) shows the resulting phase field for the same experiment. The image reveals a vortex structure with three arms (blue, red, yellow) which are pinned to a single obstacle marked with a white "x." The pattern is affected by a different wave train in the lower left-hand corner where the phase is ill defined. Most importantly, we find that the three-armed vortex in Figs. 1(a) and 1(b) has equal distances between the individual tips, thus, indicating repulsion between the different wave arms. Additional measurements show that it takes less than 2 min to establish this stable state from initially asymmetric conditions produced by the externally controlled nucleation process.

The most surprising result of our study is that the repulsion of spiral arms can give way to attraction, if the size of the obstacle is *increased*. The difference image in Fig. 2(a) shows a typical example for this anomalous size effect. Here, a counter-clockwise rotating, three-armed vortex is pinned to the obstacle located at the center of the field of view. In contrast to Fig. 1, the spiral arms are separated by two short and one very large distance, thus, forming dense pulse packets. The leading pulse segments are brighter than the closely trailing ones indicating larger changes in intensity. This increase in pulse amplitude is also observed in pseudo-one-dimensional CHDBZ media, but its origin is unknown. For the same experiment, Fig. 2(b) shows a time-space plot obtained from a square path around the central obstacle. These data unfolds the tip dynamics of the vortex and yields two short ($\lambda_{1,2}$=0.78 mm) and one large distance (λ_3 =4.33 mm). The plot also establishes that the aggregated vortex is in a stationary, stable state as the pulse velocities are identical.

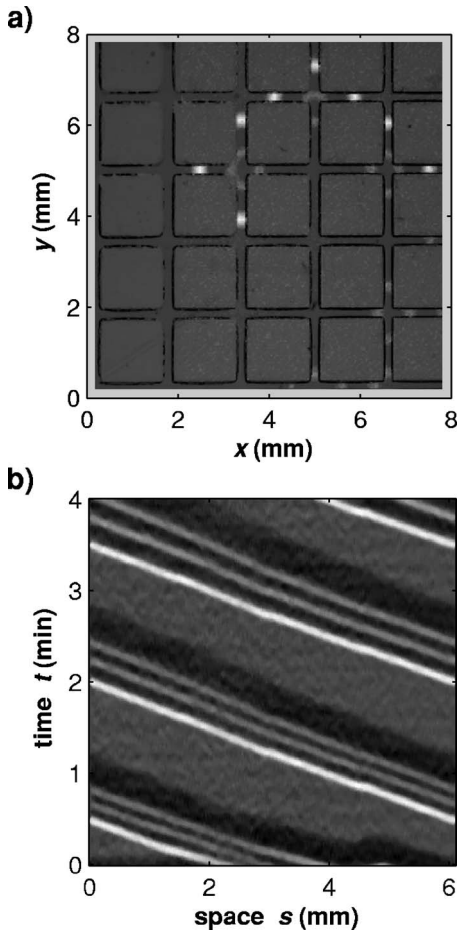

FIG. 2. (a) Difference image of a pinned three-armed spiral with attractive pulse interaction. Tips rotate counter clockwise around the central obstacle. The obstacle width is 1.5 mm. (b) Time-space plot of the same experiment illustrating the tip rotation around the central obstacle.

The size dependence of the transition from a repulsive to an attractive vortex state is illustrated in Fig. 3(a). The inset shows the wavelengths $\lambda_{1,2}$ measured for two-armed spirals as a function of obstacle perimeter U. For small obstacles,

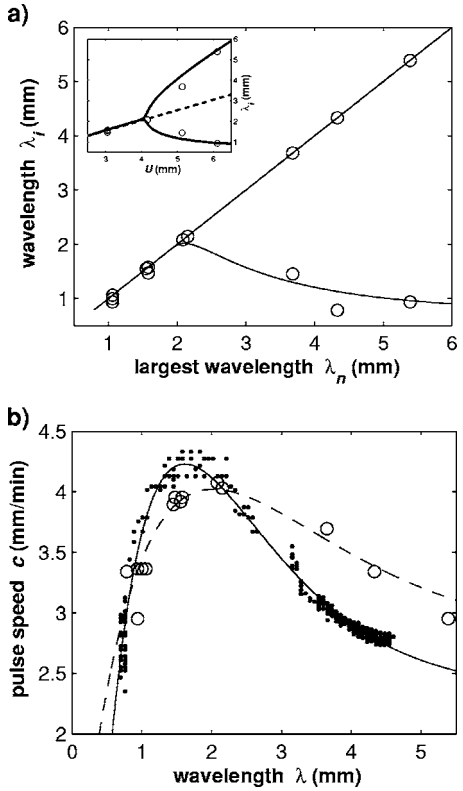

FIG. 3. (a) Bifurcation diagram for pinned n-armed spiral waves. The wavelengths are plotted in terms of the obstacle perimeter U (inset, $n=2$) and the largest wavelength λ_n (main figure, $n=2,3$). Solid and dashed lines are the stable and unstable fixed points obtained from kinematic analysis, respectively. (b) Dispersion data measured from pulse stacking in a pseudo-one-dimensional system (dots) and pinned spiral waves (circles). The solid and dashed lines are the corresponding least-squares fits using the function $c(\lambda)=c_0+\nu(\lambda-\lambda_0)\exp(-k\lambda)$ with the latter one yielding $(c_0,\nu,\lambda_0,k)=(2.95\ \mathrm{mm/min}, 3.81\ \mathrm{s}^{-1}, 0.73\ \mathrm{mm}, 0.75\ \mathrm{mm}^{-1})$.

we find $\lambda_1=\lambda_2=U/2$, thus, indicating front repulsion. For larger perimeters, the spiral arms aggregate and yield one small and one large wavelength. The bifurcation perimeter is approximately 4.1 mm and increases with increasing numbers of spiral arms n (not shown). To combine data from n-armed spirals with different values of n, we plot the measured wavelengths $\lambda_i(i=1,\ldots,n)$ versus the largest wavelength λ_n of the given set [see main part of Fig. 3(a)]. The plot reveals a bifurcation between attractive and repulsive dynamics at a λ_n value slightly above 2 mm.

The observed transition results from an overshoot anomaly of the underlying, one-dimensional dispersion relation. Figure 3(b) shows the pulse speed c as a function of interpulse distance λ. Data are measured from dynamic pulse stacking experiments in a pseudo-one-dimensional reaction system (small dots) as well as from pinned spiral waves (open circles). The two data sets differ slightly along the anomalous branch, which could be due to the nonstationary nature of the stacking pulses. The curves correspond to least-squares fits using an arbitrary but simple function. In the following, these fits are used to describe the vortex bifurcation in terms of a simple kinematic model.

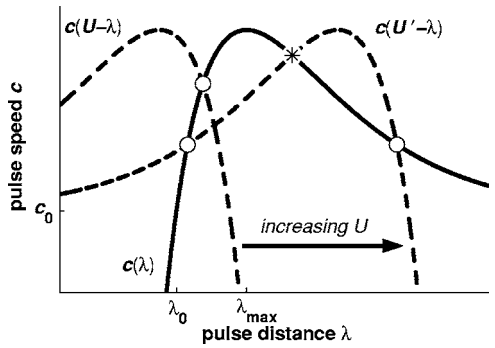

FIG. 4. Schematic drawing illustrating front aggregation in terms of a kinematic analysis. Fixed points for two different perimeters ($U<U'$) are marked as circles (stable) and star (unstable).

To understand the observed bifurcation, we focus on the motion of the spiral tips since they are the pacemaker of the global pattern. Disregarding minor, curvature-induced velocity changes at the corners of the obstacle, we can discuss a pinned, n-armed spiral as a group of n particles traveling in a one-dimensional medium with periodic boundaries. The length of this circular path equals the perimeter U of the obstacle. We also assume that the velocity c_i of the ith particle depends only on the distance to its predecessor $i+1$. In addition, the sum of all interpulse distances must equal U, since we assume infinitely thin, particle-like wave pulses. Consequently, the tip motion is described by the kinematic equations

$$\frac{ds_i}{dt}=c(s_{i+1}-s_i), \tag{1}$$

$$\frac{ds_n}{dt}=c\left[U-\sum_{i=1}^{n-1}(s_{i+1}-s_i)\right], \tag{2}$$

where $s_i(1\leqslant i\leqslant n-1)$ and s_n are the n different pulse positions. For simplicity of notation, the latter equations assume $s_{i+1}>s_i$ without the limitation of generality. Using the fit of the underlying dispersion relation [dashed line in Fig. 3(b)], these equations allow us to compute the stable stationary state(s) of the multiarmed vortex for different values of U. The corresponding results are shown in Fig. 3(a) as solid lines. They are in very good agreement with the experimental data, which indicates that front aggregation in vortices is dominated by the dispersion relation of the medium while curvature effects are negligible.

In the following, we limit our discussion to the case of two-armed spirals, but more complex structures can be analyzed in a similar fashion [9]. Stationary states must obey $c(\lambda)=c(U-\lambda)$, where λ is one of the two interpulse distances. The latter equation yields the trivial fixed point $\lambda^*=U/2$, which corresponds to the repulsive vortex state. For monotonic dispersion relations, this is the only stationary solution. For anomalous dispersion, however, other solutions can exist as in our case, where two additional fixed points appear for sufficiently large U values (see Fig. 4). This bifurcation occurs if $U/2>\lambda_{max}$, where λ_{max} is the wavelength

for which the dispersion curve has maximal pulse speed. It is accompanied by a change in stability because a fixed point λ^* is stable only if $c'(U-\lambda)+c'(\lambda)|_{\lambda=\lambda^*}>0$. Hence, the transition from a repulsive to an aggregated state is a supercritical pitchfork bifurcation.

In conclusion, we presented an experimental study of multiarmed spirals in an excitable reaction-diffusion medium. The vortices are pinned to heterogeneities and undergo a condensation-like rearrangement of their individual arms if the system size is expanded above a critical threshold. We suggest that similar phenomena can occur in biological systems for which anomalous dispersion is known to exist [14]. Consequently, spiral-arm aggregation should affect intracellular concentration waves where certain organelles might act as nonexcitable anchors. Similarly, it could be observable in cell colonies and tissues with locally compromised regions.

This work was supported by the Chemistry Division of the National Science Foundation. We thank Th. M. Fischer and H. Engel for discussions.

[1] E. Meron, Phys. Rep. **218**, 1 (1992).

[2] S. Jakubith, H. H. Rotermund, W. Engel, A. von Oertzen, and G. Ertl, Phys. Rev. Lett. **65**, 3013 (1990); H. R. Petty and A. D. Schreiber, Proc. Natl. Acad. Sci. U.S.A. **100**, 4533 (2003); S. C. Müller, T. Mair, O. Steinbock, Biophys. Chem. **72**, 37 (1998); M. A. Dahlem and S. C. Müller, Ann. Phys. **13**, 442 (2004); S. M. Hwang, K. H. Yea, and K. J. Lee, Phys. Rev. Lett. **92**, 198103 (2004).

[3] *Chemical Waves and Patterns*, edited by R. Kapral and K. Showalter (Kluwer, Dordrecht, Netherlands, 1995).

[4] O. Steinbock and S. C. Müller, Physica A **188**, 61 (1992); D. Pazo, L. Kramer, A. Pumir, S. Kanai, I. Efimor, and V. Krinsky, Phys. Rev. Lett. **93**, 168303 (2004).

[5] B. T. Ginn and O. Steinbock, Phys. Rev. Lett. **93**, 158301 (2004).

[6] J-M. Flesselles, A. Belmonte, and V. Gáspár, J. Chem. Soc., Faraday Trans. **94**, 851 (1998).

[7] C. T. Hamik, N. Manz, and O. Steinbock, J. Phys. Chem. A **105**, 6144 (2001); M. Or-Guil, I. G. Kevrekidis, and M. Bär, Physica D **135**, 154 (2000); M. Falcke, M. Or-Guil, and M. Bär, Phys. Rev. Lett. **84**, 4753 (2000); G. Bordiougov and H. Engel, Phys. Rev. Lett. **90**, 148302 (2003); N. Manz, C. T. Hamik, and O. Steinbock, Phys. Rev. Lett. **92**, 248301 (2004).

[8] A. T. Winfree, Physica D **49**, 125 (1991); C. Elphick, E. Meron, and E. A. Spiegel, Phys. Rev. Lett. **61**, 496 (1988); O. Steinbock, Phys. Rev. Lett. **88**, 228302 (2002).

[9] J. Christoph, M. Eiswirth, N. Hartmann, R. Imbihl, I. Kevrekidis, and M. Bar, Phys. Rev. Lett. **82**, 1586 (1999).

[10] C. T. Hamik and O. Steinbock, New J. Phys. **5**, 58 (2003).

[11] T. Deng, H. K. Wu, S. T. Brittain, and G. M. Whitesides, Anal. Chem. **72**, 3176 (2000).

[12] B. T. Ginn, B. Steinbock, M. Kahveci, and O. Steinbock, J. Phys. Chem. A **108**, 1325 (2004).

[13] K. Kurin-Csörgei, A. M. Zhabotinsky, M. Orbán, and I. R. Epstein, J. Phys. Chem. **100**, 5393 (1996); K. Kurin-Csörgei, A. M. Zhabotinsky, M. Orbán, and I. R. Epstein, J. Phys. Chem. A **101**, 6827 (1997).

[14] See, e.g., M. Goldermann, W. Hanke, A. C. Guimaraes de Almeida, and V. M. Fernandes de Lima, Int. J. Bifurcation Chaos Appl. Sci. Eng. **8**, 1541 (1998).